DMD Fast Forward. Published on April 4, 2018 as DOI: 10.1124/dmd.117.079830
This article has not been copyedited and formatted. The final version may differ from this version.

Title Page

Predicting anti-tumor effect of deoxypodophyllotoxin in NCI-H460 tumor-bearing mice based on in vitro pharmacodynamics and physiologically based pharmacokinetic-pharmacodynamic model

Yang Chen, Kaijing Zhao, Fei Liu, Ying Li, Zeyu Zhong, Shijin Hong, Xiaodong Liu and Li Liu

Center of Drug Metabolism and Pharmacokinetics, School of Pharmacy, China Pharmaceutical University, Nanjing, China (Y.C., K.Z., F.L., Y.L., Z.Z., S.H., X.L., L.L.)

DMD Fast Forward. Published on April 4, 2018 as DOI: 10.1124/dmd.117.079830
This article has not been copyedited and formatted. The final version may differ from this version.

Running Title Page

Running title: Predicting in vivo anti-tumor effect of DPT by PBPK-PD model

Correspondence to:

Li Liu (liulee@yeah.net) and Xiaodong Liu (xdliu@cpu.edu.cn)

Phone: +86 25 8327 1006; Fax: +86 25 8327 1060;

Center of Drug Metabolism and Pharmacokinetics, School of Pharmacy, China Pharmaceutical University, No.24 Tongjia Lane, Nanjing 210009, China.

Statistics:

The number of text pages: 43

The number of tables: 3

The number of figures: 7

The number of references: 37

The number of words in Abstract: 250

The number of words in Introduction: 698

The number of words in Discussion: 1486

Abbreviations:

$AUC_{0\text{-}tn}$, area under the concentration-time curve from time zero to last time; $AUC_{0\text{-}\infty}$, area under the concentration-time curve from time zero to infinity; CCK-8, enhanced cell counting kit-8; CL,

DMD Fast Forward. Published on April 4, 2018 as DOI: 10.1124/dmd.117.079830
This article has not been copyedited and formatted. The final version may differ from this version.

clearance; C_{max}, the maximum concentration; CV, coefficient of variation; DPT, deoxypodophyllotoxin; CYP, cytochrome P450; E_{max}, the maximum effect; EC_{50}, concentration for 50% of maximum effect; f_u, unbound fraction in plasma; IC_{50}, concentration for 50% of inhibition effect; K_m, Michaelis-Menten constant; $K_{p,T}$, tissue-to-plasma concentration ratio; LC-MS/MS, liquid chromatography-tandem mass spectrometry; PBPK, physiologically based pharmacokinetic; PBPK-PD, physiologically based pharmacokinetic-pharmacodynamic; PBSF, physiological-based scaling factor; PK-PD, pharmacokinetic-pharmacodynamic; PS, permeability-surface product; $t_{1/2}$, terminal half-life; V_{max}, the maximum metabolic velocity; V_{ss}, apparent volume of distribution at steady state; γ, Hill coefficient.

DMD Fast Forward. Published on April 4, 2018 as DOI: 10.1124/dmd.117.079830
This article has not been copyedited and formatted. The final version may differ from this version.

Abstract

Anti-tumor evaluation in tumor-bearing mouse is time- and energy-consuming. We aimed to investigate whether in vivo anti-tumor efficacy could be predicted based on in vitro pharmacodynamics using deoxypodophyllotoxin (DPT), a developing anti-tumor candidate, as a model compound. Proliferation kinetics of monolayer cultivated NCI-H460 cells under various DPT concentrations was quantitatively investigated accompanied by calibration curves. Koch's two-phase natural growth model combined with sigmoid E_{max} model, i.e. $dM/dt=2\lambda_0\lambda_1 M/(\lambda_1+2\lambda_0 M)-E_{max}C^{\gamma}/(EC_{50}{}^{\gamma}+C^{\gamma})\cdot M$, was introduced to describe cell proliferation (M) against time under DPT treatment (C). Estimated in vitro pharmacodynamic parameters were: EC_{50}, 8.97 nM; E_{max}, 0.820 day^{-1} and γ, 7.13. A physiologically based pharmacokinetic (PBPK) model including tumor compartment was introduced, which could predict DPT disposition in plasma, tumor tissue and main normal tissues of NCI-H460 tumor-bearing mice following single dose. In vivo pharmacodynamic model and parameters were assumed the same as in vitro ones, and linked with simulated tumor pharmacokinetic profiles by PBPK model, to build a physiologically based pharmacokinetic-pharmacodynamic (PBPK-PD) model. After estimating natural growth parameters (λ_0 and λ_1), we desirably predicted the tumor growth in NCI-H460 tumor-bearing mice during multi-dose DPT treatment, both in this study and literature, by the PBPK-PD model. The model was further successfully applied to predict tumor growth in SGC-7901 tumor-bearing mice. These data indicated that in vivo anti-tumor efficacy might be predicted based on in vitro cytotoxic assays via PBPK-PD model approach. The approach was demonstrated reasonable and applicable, which might facilitate and accelerate anti-cancer candidate screening and dose regimen design in drug discovery process.

DMD Fast Forward. Published on April 4, 2018 as DOI: 10.1124/dmd.117.079830
This article has not been copyedited and formatted. The final version may differ from this version.

Introduction

Deoxypodophyllotoxin (DPT) is one of main active ingredients in herbs like *Podophyllum emodi*, *Anthriscus sylvestris* and *Pulsatilla koreana* (Khaled et al., 2013; Wong et al., 2000). The lignan compound exhibits various pharmacological activities such as anti-tumor, anti-viral, anti-platelet aggregation and anti-inflammatory effects (Khaled et al., 2013), among which the anti-tumor effect is the most attractive and widely characterized (Hu et al., 2016; Jiang et al., 2013; Khaled et al., 2016; Kim et al., 2002; Shin et al., 2010). In China, a phase I clinical trial for DPT has been approved towards patients of lung cancer, gastric cancer and breast cancer, especially the ones resistant to paclitaxel and etoposide, in an intravenous formulation of β-cyclodextrin inclusion complex.

Several studies have demonstrated that DPT strongly exerts its cytotoxic effect via inhibiting polymerization and promoting depolymerization of tubulin, as well as inducing cell cycle arrest at G2/M phase accompanied by cell apoptosis (Guerram et al., 2015; Khaled et al., 2013; Yong et al., 2009). In vitro experiments demonstrated that IC_{50} values of DPT against several human cancer cell lines were in the low nanomolar range (13~27 nM), far superior to its analog etoposide (Guerram et al., 2015). Several studies also revealed that the inhibition to specific cell lines by DPT was exposure time- and concentration-dependent (Jiang et al., 2013; Wang et al., 2015; Yong et al., 2009). Furthermore, in vivo anti-tumor effects of DPT have been illustrated (Khaled et al., 2016; Wang et al., 2015; Wu et al., 2013).

Our previous studies have showed the metabolic kinetics of DPT in hepatic microsomes and its high plasma protein binding in various species (Chen et al., 2016; Xie et al., 2016). Demethylenated metabolite (M2) is the main metabolite of DPT (Chen et al., 2016; Xie et al., 2016). Subsequently, a whole body physiologically based pharmacokinetic (PBPK) model of DPT including main organs of

body was established based on the in vitro assays (Chen et al., 2016). The developed PBPK model successfully predicted plasma pharmacokinetics of DPT in mice, rats, monkeys and dogs. Good predictions were also found with regard to pharmacokinetics in tissues of mice (Chen et al., 2016). It is possible to gain a profound understanding of the dynamics of drug disposition in both plasma and tissues/organs through PBPK model. Thus making connections between drug exposure in target tissues and its efficacy is facilitated.

Mouse xenograft model of human tumor is an important pharmacological model and essential for anti-tumor evaluation prior to clinical trials (Kelland, 2004; Ruggeri et al., 2014). Tumor growth inhibition is the most direct and decisive standard for the efficacy evaluation, and easy to be quantified continuously. Nevertheless, the experiments related to tumor-bearing mouse are time-, economy- and energy-consuming. In vitro evaluation on monolayer cultured cell proliferation is much more convenient, economical and reproducible compared with in vivo study. Therefore, it will be meaningful to predict the anti-tumor effect in tumor-bearing mouse based on in vitro assays. Even though in vitro data may not interpret in vivo efficacy directly, intrinsic links may exist between in vitro and in vivo pharmacodynamic characteristics. The aim of present study was to forecast in vivo efficacy based on in vitro approach through PBPK-PD model establishment, using DPT as a model compound. In vitro proliferation kinetics of NCI-H460 cells (a human non-small cell lung cancer), a sensitive cell line (Wu et al., 2013), was investigated under different DPT concentrations. Then in vitro pharmacodynamic models were established and corresponding parameters were estimated. Concentration-time profiles of DPT in plasma, tumor tissue and normal tissues of NCI-H460 tumor-bearing mice were simultaneously predicted using a developed PBPK model with tumor tissue compartment and further validated by in vivo data. Finally, a physiologically based

DMD Fast Forward. Published on April 4, 2018 as DOI: 10.1124/dmd.117.079830
This article has not been copyedited and formatted. The final version may differ from this version.

pharmacokinetic-pharmacodynamic (PBPK-PD) model was developed based on in vitro pharmacodynamic model and parameters, as well as simulated pharmacokinetic profiles in tumor tissue, to predict anti-tumor effects of DPT in NCI-H460 tumor-bearing mice. The predictions were validated by tumor volume growth data during DPT treatment. In addition, this approach was further confirmed by its application in SGC-7901 (a human gastric cancer) tumor model. The possibility was expected that perturbed tumor growth could be predicted by extrapolating in vitro pharmacodynamics to in vivo circumstance using PBPK-PD model.

DMD Fast Forward. Published on April 4, 2018 as DOI: 10.1124/dmd.117.079830
This article has not been copyedited and formatted. The final version may differ from this version.

Materials and Methods

Materials

The analytical standards of DPT (purity 99.88%, for in vitro and analytical studies), its metabolite M2 (purity 99.45%) and β-cyclodextrin inclusion complex of DPT (content 3.36%, for in vivo administrations) were kindly provided by Medicinal and Chemical Institute of China Pharmaceutical University (Nanjing, China). Diazepam (purity 99.9%) used as internal standard was purchased from National Institutes for Food and Drug Control (Beijing, China). Enhanced cell counting kit-8 (CCK-8, #C0042) and BCA Protein Assay Kit (#P0012) were purchased from Beyotime Institute of Biotechnology (Nantong, China). Cell culture media, fetal bovine serum, 0.25% trypsin and rapid equilibrium dialysis device system (12K MWCO, #90112) were purchased from Thermo Fisher Scientific (Waltham, MA, USA). All the other reagents were commercially available.

NCI-H460 cell culture and in vitro pharmacodynamic assay of DPT

NCI-H460 cell line was provided by Type Culture Collection of Chinese Academy of Sciences (Shanghai, China), which has been authenticated by short tandem repeat analysis. Cells were cultured in RPMI-1640 medium (Gibco^{TM}, #31800022) supplemented with 1.5 g/L $NaHCO_3$, 2.5 g/L glucose, 0.11 g/L sodium pyruvate, antibiotics (62.5 mg/L ampicillin and 100 mg/L streptomycin) and 10% fetal bovine serum (Gibco^{TM}, #10100147), maintained in humidified atmosphere containing 5% CO_2 at 37 ℃.

Calibration curves for cell counts were established as follows. The cultured cells were digested and resuspended by cell medium. Then the cell suspension was counted by TC10^{TM} automated cell counter (Bio-rad, Hercules, CA, USA) and further diluted for a series of working suspensions with

DMD Fast Forward. Published on April 4, 2018 as DOI: 10.1124/dmd.117.079830
This article has not been copyedited and formatted. The final version may differ from this version.

known cell count density (1×10^4~1×10^6 cells/mL) by the medium. An aliquot of each working suspension (100 μL) was seeded in a 96-well plate and cells were allowed to attach (for about 4 h). Medium was then gently aspirated and 100 μL no phenol red RPMI-1640 medium (Gibco™, #11835030) and 10 μL CCK-8 reagent were added to each well. The plate was subsequently placed in cell incubator for 1 h. The absorbance of each well was obtained at wavelength of 450 nm by microplate reader (Bio-tek, Winooski, VT, USA) and calibration curve was established by the regression of absorbances to cell counts in the wells.

For pharmacodynamic assay, NCI-H460 cells were seeded in 96-well plates at a density of 1000 cells/well and allowed to attach for 24 h. Then cells were treated with 100 μL either vehicle (RPMI-1640 medium) or medium containing different concentrations of DPT (5.53, 7.29, 9.80, 13.06 and 17.59 nM) for designed times (0, 12, 24, 36, 48, 60, 72 and 84 h). Cell counts after treatments were measured by accompanied calibration curves and the proliferation profiles against time under different DPT exposures were obtained.

In vitro pharmacodynamic model development

DPT exerts its cytotoxic effect on NCI-H460 cells by triggering necroptosis according to a previous report (Wu et al., 2013). We assumed that cells in different phases in cell cycle were affected by the compound to the same extent. Therefore a cell cycle non-specific cytotoxicity model was used to depict the in vitro cell proliferation kinetics exposed to DPT (Lobo and Balthasar, 2002):

$$\frac{dM}{dt} = (k_{ng} - K) \times M \quad (1)$$

where M stands for cell count. The proliferation rate is composed of the natural growth and drug effect according to the model. k_{ng} and K stand for the first-order kinetic parameters (unit: day^{-1}) of the

DMD Fast Forward. Published on April 4, 2018 as DOI: 10.1124/dmd.117.079830
This article has not been copyedited and formatted. The final version may differ from this version.

two parts above, respectively.

Nevertheless, the exponential equation above might not be suitable for being extended to predict in vivo tumor growth, which usually demonstrates a two-phase growth feature: an initial exponential growth and a following linear growth (Koch et al., 2009). Therefore, in order to match in vivo circumstance and achieve in vitro-in vivo extrapolation, the natural proliferation of cultured cells without drug perturbation was also described by the two-phase growth model suggested by Koch et al.(Koch et al., 2009):

$$\frac{dM}{dt} = \frac{2\lambda_0\lambda_1 M}{\lambda_1 + 2\lambda_0 M} \tag{2}$$

where M represents cell count. λ_0 (unit: day^{-1}) and λ_1 (unit: count/day) represent exponential and linear proliferation rate parameters, respectively, and could be obtained by fitting the model to natural cell proliferation data.

When cell proliferation was affected by drug treatment, an inhibitive rate was added to equation 2 (Eigenmann et al., 2016; Yuan et al., 2015) :

$$\frac{dM}{dt} = \frac{2\lambda_0\lambda_1 M}{\lambda_1 + 2\lambda_0 M} - K \cdot M \tag{3}$$

where K stands for the first-order inhibitive parameter (unit: day^{-1}).

DPT exhibits a sigmoid E_{max} pharmacodynamic characteristic against NCI-H460 cell line in the previous study (Wu et al., 2013). Accordingly, K in equation 1 and 3 could be expressed as follows:

$$K = \frac{E_{max} \times C^{\gamma}}{EC_{50}^{\gamma} + C^{\gamma}} \tag{4}$$

where C represents DPT concentration (unit: nM), while E_{max} (unit: day^{-1}), EC_{50} (unit: nM) and γ are the in vitro pharmacodynamic parameters of DPT.

Both the two models (equation 1 and 3) were fitted to the cell proliferation profiles obtained

above respectively and corresponding in vitro parameters were estimated.

Tumor xenograft model

BALB/$c^{nu/nu}$ nude mice (half males and half females) were purchased from Cavens Lab Animal Co., Ltd. (Changzhou, China). The animals were housed in specific pathogen free environment under constant temperature (25~28 ℃) and humidity (50~60%), with 12 h light/dark cycle. Rodent chow and water were autoclaved and provided *ad libitum*. Animal experiments were carried out according to the Guide for the Care and Use of Laboratory Animals and approved by Animal Ethics Committee of China Pharmaceutical University, No. CPU-PCPK-14311010078.

The nude mice of about 4~6 weeks age (weighed 18~22 g) were inoculated with tumor cell suspension subcutaneously (2×10^6 cells/mouse) in the right flank region. Tumor diameters from two perpendiculars (a, length; b, width) were measured by a vernier caliper and tumor volume (V, unit: cm^3) was calculated according to the equation: $V = (a\times b^2)/2$. (Magni et al., 2006; Salphati et al., 2010)

Pharmacokinetic study in NCI-H460 tumor-bearing mice

When the mean tumor volume reached 500 mm^3, 108 mice were randomly divided into two groups and received single dose of DPT of 6.25 or 25 mg/kg via tail veins, respectively. The mice were fasted overnight prior to dosing. DPT in β-cyclodextrin inclusion complex was dissolved in 0.9% normal saline within 2 h before administration. Six mice (three males and three females) from each group were sacrificed at 2, 5, 10, 20, 45, 60, 120, 240 and 480 min post-dose, respectively. For each mouse blood sample was collected into heparinized tube and centrifuged for 5 min at 8000 *g* to obtain plasma. Tumor tissues were simultaneously removed and weighed. Distributions of DPT in heart, liver, lung,

DMD Fast Forward. Published on April 4, 2018 as DOI: 10.1124/dmd.117.079830
This article has not been copyedited and formatted. The final version may differ from this version.

kidney, brain, muscle and intestine of tumor-bearing mice at 5, 20, 60 and 120 min following intravenous dose (25 mg/kg) were also investigated. The tissues including tumors were homogenized in pure water (1:5, w/v). The plasma and tissue homogenate samples were stored at -70 ℃ until analysis, in which DPT concentrations were measured by an LC–MS/MS method previously described (Liu et al., 2016).

Another eight tumor-bearing mice without DPT administration were sacrificed for blank plasma and liver. Hepatic microsomes were prepared according to a procedure previously described (Chen et al., 2011). Blank plasma from the eight mice was pooled for the protein binding study. The hepatic microsomes and plasma were also kept at -70 ℃ until use.

M2 is main metabolite of DPT in hepatic microsomes of mouse, rat, monkey, dog and human (Chen et al., 2016; Xie et al., 2016). Preliminary experiment also showed that for 200 nM of DPT following 15-min incubation in liver microsomes of NCI-H460 tumor-bearing mice (0.05 mg protein/mL), 80.3% of the disappeared DPT was metabolized to M2. Therefore kinetic parameters of M2 formation from DPT in hepatic microsomes were investigated to characterize DPT metabolism in tumor-bearing mice. The composition of microsomal incubation mixture and incubation procedure were the same as the previous report (Xie et al., 2016). A series of DPT concentrations (0.0471~3.02 μM) were used. Microsomal protein level and incubation time were set to be 0.01 mg/mL and 5 min, respectively. M2 formation in the incubation system was measured based on a previously described method (Xie et al., 2016). Metabolic kinetic parameters of M2 formation were estimated for each animal individual.

Plasma protein binding of DPT in tumor-bearing mouse was evaluated by a method previously described using rapid equilibrium dialysis device (Chen et al., 2016). Initial DPT concentration in

DMD Fast Forward. Published on April 4, 2018 as DOI: 10.1124/dmd.117.079830
This article has not been copyedited and formatted. The final version may differ from this version.

plasma was set to be 1.0 μg/mL. Evaluations were carried out in triplicate.

PBPK model development

A whole body PBPK model of DPT for tumor-bearing mouse was constructed as the same scheme in the previous report (Chen et al., 2016) except that a tumor compartment was included (Figure 1). The body weight of tumor-bearing mouse was assumed to be 20 g. Volume and blood flow rate of each normal organ compartment of tumor-bearing mouse were considered the same as normal mouse (Chen et al., 2016) (Table 1). It was assumed that DPT was mainly eliminated in liver via transforming to M2 and disposition of DPT in most tissues was illustrated by perfusion-rate limited model. The detailed differential equations in normal tissues were described in "Supplemental methods".

An assumption that unbound tissue-to-plasma concentration ratio of DPT was identical across species have given good predictions for pharmacokinetics in various species (Chen et al., 2016). Thus, tissue-to-plasma concentration ratio ($K_{p,T}$) values of DPT in normal tissues of tumor-bearing mouse were derived from those of rats ($K_{p,T,\,rat}$) by the equation: $K_{p,T} = K_{p,T,\,rat} \times f_u / f_{u,\,rat}$, where f_u and $f_{u,\,rat}$ are unbound fractions of DPT in plasma of tumor-bearing mouse and rat, respectively. $K_{p,T,\,rat}$ and $f_{u,\,rat}$ were cited from our previous study (Chen et al., 2016). Calculated $K_{p,T}$ values of tumor-bearing mouse were summarized in Table 1.

Pharmacokinetic profiles of DPT in plasma, tumor and main normal tissues were predicted by the developed PBPK model and corresponding pharmacokinetic parameters of predicted profiles were also estimated by non-compartmental analysis. Then the predictions were compared with observed data to validate the model. Accuracy of prediction was evaluated by fold-error (Chen et al., 2016).

DMD Fast Forward. Published on April 4, 2018 as DOI: 10.1124/dmd.117.079830
This article has not been copyedited and formatted. The final version may differ from this version.

Predicted value within twofold error of observed value was considered to be acceptable (Guest et al., 2011; Parrott et al., 2005).

In vivo pharmacodynamics prediction by PBPK-PD model

DPT concentration profiles in tumor tissue of tumor-bearing mice during multiple doses treatment were simulated using the validated PBPK model. The profiles were further connected to in vitro pharmacodynamics of DPT and the characteristics of tumor natural growth to predict the anti-tumor effect in NCI-H460 tumor-bearing mice. In vitro evaluation on NCI-H460 cell line also showed that the main metabolite M2 had no anti-tumor effect (IC_{50} > 100 μM, 72h), indicating that the anti-tumor effect was mainly attributed to DPT.

Tumor growth with drug intervention was illustrated by both equation 5 and 6, which were similar to equation 1 and 3 describing in vitro pharmacodynamics of DPT respectively:

$$\frac{dV}{dt} = k_{ng} \times V - \frac{E_{max} \times C_f^{\gamma}}{EC_{50}^{\gamma} + C_f^{\gamma}} \times V \quad (5)$$

$$\frac{dV}{dt} = \frac{2\lambda_0 \lambda_1 V}{\lambda_1 + 2\lambda_0 V} - \frac{E_{max} \times C_f^{\gamma}}{EC_{50}^{\gamma} + C_f^{\gamma}} \times V \quad (6)$$

where V represents tumor volume (unit: mL). k_{ng} (unit: day^{-1}) represents exponential natural growth parameter. λ_0 (unit: day^{-1}) and λ_1 (unit: mL/day) represent exponential and linear growth rate parameters of natural growth, respectively. The two equations were fitted to tumor volume growth data without DPT treatment respectively to get in vivo k_{ng}, λ_0 and λ_1. Values of in vivo pharmacodynamic parameters E_{max} (unit: day^{-1}), EC_{50} (unit: nM) and γ of DPT were assumed to equal corresponding in vitro estimated values. C_f is free DPT concentration (unit: nM) in tumor tissue and could be simulated dynamically by PBPK model. Consequently, tumor volume growth curves against

DMD Fast Forward. Published on April 4, 2018 as DOI: 10.1124/dmd.117.079830
This article has not been copyedited and formatted. The final version may differ from this version.

time during DPT treatment could be obtained by solving the differential equations in PBPK-PD model.

All mathematical models above were coded and solved by Phoenix WinNonlin software (version 7.0, Certara, Co., Princeton, NJ, USA). Parameter estimations were also conducted on the software.

Validation of pharmacodynamics prediction in NCI-H460 tumor-bearing mice

As tumor volumes reached about 100 mm^3, eighteen tumor-bearing mice were randomized into three groups (three males and three females in each group), namely vehicle control, 6.25 mg/kg DPT and 25 mg/kg DPT treatment groups. DPT or vehicle was administered via tail veins every three days for eight doses in total. Body weights and tumor volumes were measured every other day. The day of first administration was designated as time zero. Predicted tumor growth curves during DPT treatment by the developed PBPK-PD model were compared to the observations. Predictive fold-error within two denoted success.

Another dataset from a previous report (Wu et al., 2013) was used to further validate the developed PBPK-PD model. Doses of DPT were set to be 5, 10 and 20 mg/kg, respectively, which were administered to NCI-H460 tumor-bearing mice three times a week. λ_0 and λ_1 values were also estimated using tumor growth curve of vehicle control group. Tumor growth curves during DPT treatment were predicted by the developed PBPK-PD model and validated by reported observations (Wu et al., 2013).

PBPK-PD model application in SGC-7901 tumor-bearing mice

The developed PBPK-PD model was further applied to predict the anti-tumor effect of DPT in SGC-7901 tumor-bearing mice. SGC-7901 cell line was provided by Type Culture Collection of Chinese Academy of Sciences (Shanghai, China) and cultured as described above. For in vitro pharmacodynamic studies, SGC-7901 cells were seeded in 96-well plates at a density of 3000 cells/well and allowed to attach for 24 h. Then cells were treated with 100 μL either vehicle (RPMI-1640 medium) or the medium containing different concentrations of DPT (2.57, 3.22, 4.02, 5.02 and 6.28 nM) for designed times (0, 12, 24, 36, 48, 60, 72 and 84 h). Cell counts were measured using calibration curves of SGC-7901 cells. Corresponding in vitro pharmacodynamic parameters of DPT were estimated using the Koch's two-phase model combined with sigmoid E_{max} model (equation 3).

It was assumed that PBPK model structure and parameters of DPT were the same in SGC-7901 and NCI-H460 tumor-bearing mouse. The concentration profiles of DPT in tumor and plasma of SGC-7901 tumor-bearing mouse were predicted and compared with observed data following single intravenous dose of DPT (6.25 mg/kg). Eighteen male SGC-7901 tumor-bearing mice were randomly divided into six time groups, which were sacrificed at 6, 20, 30, 60, 120, 480 min post-dose, respectively. Plasma and tumor samples were obtained, in which DPT concentrations were measured as described above.

In vivo anti-tumor effect data of DPT in SGC-7901 tumor-bearing mice were cited from a previous report (Wang et al., 2015). The mice were intravenously given vehicle, 5, 10 and 20 mg/kg of DPT (three times a week) respectively and tumor volumes were measured for 17 days. λ_0 and λ_1 values for SGC-7901 tumor growth were estimated using tumor growth curve of vehicle group. Based on the combination of predicted tumor concentration profiles and estimated in vitro pharmacodynamic

DMD Fast Forward. Published on April 4, 2018 as DOI: 10.1124/dmd.117.079830
This article has not been copyedited and formatted. The final version may differ from this version.

parameters, tumor growth profiles in SGC-7901 tumor-bearing mice during DPT treatment were predicted by the PBPK-PD model and compared with reported observations (Wang et al., 2015).

DMD Fast Forward. Published on April 4, 2018 as DOI: 10.1124/dmd.117.079830
This article has not been copyedited and formatted. The final version may differ from this version.

Results

In vitro pharmacodynamics of DPT against NCI-H460 cell line

To quantify cell counts, calibration curves were established on five consecutive days with desirable precision as $y = (0.0951 \pm 0.0083)\ x - (0.0030 \pm 0.0038)$ (r^2>0.9918), where y and x stand for absorbance and cell count ($\times 10^4$), respectively (Figure 2). The proliferation of NCI-H460 cells against time under different concentrations of DPT was depicted in Figure 3. The results showed that DPT concentration-dependently exerted its potent cytotoxic effect on the tumor cell line. A sharp concentration-effect relationship was observed, which obeyed sigmoid E_{max} model. DPT scarcely exhibited its cytotoxic effect at 5.53 nM, but at 13.06 nM the maximum effect was nearly reached and proliferation was almost inhibited thoroughly. Both cell cycle non-specific cytotoxicity model (model A, equation 1) and the cytotoxicity model extended from two-phase Koch model (model B, equation 3) were fitted to the cell proliferation curves (Figure 3). Estimated in vitro pharmacodynamic parameters of the two models were listed in Table 2.

It could be seen from Figure 3 and Table 2 that both models seemed to well characterize the cell proliferation, and similar estimated results were obtained. The estimated EC_{50} values coincided with the values previously reported (Wu et al., 2013). Therefore both models along with their pharmacodynamic parameters were attempted to forecast in vivo tumor growth.

Pharmacokinetics of DPT in NCI-H460 tumor-bearing mice

DPT showed high affinity to plasma protein of tumor-bearing mouse. The evaluated protein binding value using a rapid equilibrium dialysis approach was 95.12±0.42 %, which was slightly lower than that in normal mouse (97.17±0.25 %) (Chen et al., 2016).

DMD Fast Forward. Published on April 4, 2018 as DOI: 10.1124/dmd.117.079830
This article has not been copyedited and formatted. The final version may differ from this version.

The kinetic profiles of M2 formation from DPT in hepatic microsomes of tumor-bearing mice were studied, which obeyed typical Michaelis-Menten kinetics judged by corresponding Eadie-Hofstee plots. The estimated V_{max}, K_m and calculated intrinsic clearance (CL_{int} = V_{max} / K_m) were 1.22±0.55 nmol/min/mg protein, 0.32±0.06 μM and 4.07±2.19 mL/min/mg protein, respectively (n=8). The calculated intrinsic clearance in hepatic microsomes from tumor-bearing mice was higher than that from normal mice (1.89 mL/min/mg protein) (Xie et al., 2016).

Pharmacokinetic profiles of plasma, tumor and normal tissues in tumor-bearing mice were obtained following single intravenous dose of DPT. The results showed that in plasma DPT was eliminated rapidly following administration, with a half-life of about 50 min (Figure 4A and Table 3). In tumor DPT concentration reached its peak rapidly, but its elimination was slower than that in plasma, with half-lives of 157 and 205 min (Figure 4B and Table 3). The exposure of DPT in tumor was about four times higher than that in plasma (Table 3), demonstrating that high affinity existed between the drug molecule and tumor tissue. In addition, DPT showed very high plasma clearances (2.73 and 2.77 mL/min, Table 3) exceeding liver blood flow rate (1.94 mL/min, Table 1), indicating the existence of extrahepatic elimination.

PBPK model validation in NCI-H460 tumor-bearing mice

As mentioned above, extrahepatic elimination might occur somewhere, so an additional clearance (CL_{other}) was introduced into the venous compartment of PBPK model (Figure 1). CL_{other} was calculated as the following equation based on a well-stirred model:

$$CL_{other} = CL_{in\ vivo} - \frac{Q \times f_u \times (V_{max} / K_m) \times PBSF}{Q + f_u \times (V_{max} / K_m) \times PBSF} \quad (7)$$

where $CL_{in\ vivo}$ is the in vivo clearance estimated by plasma pharmacokinetic profile following

intravenous dose of DPT (6.25 mg/kg), whose value was 2.73 mL/min (Table 3). Q is liver blood flow rate (1.94 mL/min, Table 1). f_u, PBSF, V_{max} and K_m are unbound fraction of DPT in plasma, total hepatic microsomal protein amount (49.28 mg protein/mouse, assuming the same as normal mice (Chen et al., 2016)) and kinetic parameters of M2 formation from DPT in hepatic microsomes of tumor-bearing mice, respectively. Therefore, CL_{other} was calculated to be 1.11 mL/min.

Pharmacokinetic study showed that DPT concentration-time profiles in tumor tissue did not synchronize with those in plasma, exhibiting an obvious increase before elimination. Therefore, permeability-limited model was adopted for illustrating disposition of DPT in tumor tissue as follows:

$$V_a \frac{dC_a}{dt} = Q_{Tumor} \times (C_A - C_a) - PS_{Tumor}(C_a - C_b / K_{p,Tumor}) \quad (8)$$

and

$$V_b \frac{dC_b}{dt} = PS_{Tumor} \times (C_a - C_b / K_{p,Tumor}) \quad (9)$$

where subscript a and b represent vascular and extravascular compartment, which were assumed to account for 10 and 90% of the total tumor volume (0.5 mL), respectively (Zhang et al., 2013). C (unit: nM) and V (unit: mL) are DPT concentration and volume of related compartment, respectively. C_A (unit: nM) means the drug concentration in arterial blood compartment. Tumor-to-plasma concentration ratio of DPT ($K_{p,Tumor}$) was 4.23, calculated from the $AUC_{0-\infty}$ ratio between tumor tissue and plasma of 6.25 mg/kg dose group (Table 3). Permeability-surface product of tumor (PS_{Tumor}) was estimated to be 0.0116 mL/min (CV: 9.48%) by fitting the model to tumor concentration-time profile of 6.25 mg/kg dose group, which was successfully validated by the profile of 25 mg/kg dose group. Blood flow rate of tumor (Q_{Tumor}) was assumed to be 0.14 mL/min (Zhang et al., 2013), and cardiac output of tumor-bearing mouse was set to be the sum of blood flow rates of all organs including tumor (Table 1).

DMD Fast Forward. Published on April 4, 2018 as DOI: 10.1124/dmd.117.079830
This article has not been copyedited and formatted. The final version may differ from this version.

Pharmacokinetic profiles of DPT in plasma and tumor tissue of tumor-bearing mice following single intravenous dose of DPT (6.25 and 25 mg/kg) were predicted using the developed PBPK model and compared with the observed data. Acceptable results were obtained that most of predicted concentrations and all corresponding pharmacokinetic parameters of the predicted profiles fell within twofold error of observed values (Figure 4C and Table 3).

Concentration-time profiles of DPT in main normal tissues of tumor-bearing mice following single intravenous dose of DPT (25 mg/kg) were simultaneously predicted by PBPK model and compared with observed data. The area under concentration-time curve from zero to 120 min ($AUC_{0\text{-}120min}$) in tissues was also estimated. The results showed that predicted $AUC_{0\text{-}120min}$ of DPT in main normal tissues were within twofold error of observations except lungs (Figure 5).

The validations by profiles of plasma, tumor and normal tissues showed that the developed PBPK model could predict DPT disposition in tumor-bearing mice following single intravenous dose. It indicated that DPT concentration profile in tumor tissue during multi-dose treatment might also be simulated accurately by the model.

Validation of pharmacodynamics prediction in NCI-H460 tumor-bearing mice

Perturbed tumor growth curves by DPT in NCI-H460 tumor-bearing mice were predicted by the established PBPK-PD model. During DPT treatment, tumor volume was an increasing variable against time instead of a fixed value. Accordingly, blood flow rate and permeability-surface product of tumor were assumed to be proportional to tumor volume. Body weight of mouse (regardless of tumor weight) and other parameters in PBPK-PD model were assumed constant as tumor volume increased. C_f (free DPT concentration in tumor tissue, unit: nM) was obtained by the equations C_f =

DMD Fast Forward. Published on April 4, 2018 as DOI: 10.1124/dmd.117.079830
This article has not been copyedited and formatted. The final version may differ from this version.

$f_{u,tumor} \times C_{tumor}$ and $f_{u,tumor} = f_u / K_{p,tumor}$ (Maurer et al., 2005), where C_{tumor}, $f_{u,tumor}$, f_u and $K_{p,tumor}$ are DPT concentration in tumor tissue (extravascular compartment, unit: nM), unbound fraction of DPT in tumor tissue and in plasma, and tumor-to-plasma concentration ratio of DPT, respectively. C_{tumor} was simulated dynamically by the PBPK model above.

In vivo studies demonstrated the significant anti-tumor effect of DPT in a dose-dependent manner (Figure 6A and 6B). In vivo tumor growth profiles in the present study were predicted using both equation 5 and 6, respectively (Supplemental Figure). The results showed that two-phase Koch model (equation 6) better simulated tumor growth than exponential model (equation 5) with lower AIC values (-40.3 versus -12.9 for 6.25 mg/kg; -51.5 versus -21.9 for 25.0 mg/kg) and a higher correlation coefficient (R: 0.9912 versus 0.9437). Therefore, Koch's two-phase natural growth model combined with sigmoid E_{max} model (equation 6) was selected as the final model to characterize in vitro pharmacodynamics as well as predict in vivo pharmacodynamics of DPT.

In equation 6, kinetic parameters λ_0 and λ_1 in Figure 6A were estimated to be 0.110 day^{-1} (CV: 26.8%) and 0.0797 mL/day (CV: 16.3%), respectively, by tumor growth curve of vehicle control group. Tumor growth curves in Figure 6A during DPT treatment (6.25 and 25 mg/kg, once every three days) were predicted by the developed PBPK-PD model and compared with observations. Predicted curves were in good accordance with the observed data (Figure 6A). Data previously reported (Figure 6B, Wu et al., 2013) were also used to validate the developed PBPK-PD model, of which λ_0 and λ_1 were estimated to be 0.426 day^{-1} (CV: 22.5%) and 0.142 mL/day (CV: 8.64%), respectively, by tumor growth curve of vehicle control group in Figure 6B. Acceptable prediction of tumor growth curves in Figure 6B during DPT treatment (5, 10 and 20 mg/kg, three times a week) was also obtained. Predictive fold-errors of tumor volumes in both datasets were all less than 2 (Figure 6C&D).

DMD Fast Forward. Published on April 4, 2018 as DOI: 10.1124/dmd.117.079830
This article has not been copyedited and formatted. The final version may differ from this version.

Successful validations by external data from multifaceted sources indicated the predictive accuracy and rationality of the developed PBPK-PD model.

PBPK-PD model application in SGC-7901 tumor-bearing mice

Koch's two-phase natural growth model combined with sigmoid E_{max} model was also used to characterize the in vitro proliferation profiles of SGC-7901 cells under DPT exposure (Figure 7A). The estimated in vitro pharmacodynamic parameters were: λ_0: 0.341 day^{-1} (CV: 16.4%); λ_1: 46296 count/day (CV: 52.1%); EC_{50}: 6.23 nM (CV: 13.1%); E_{max}: 1.02 day^{-1} (CV: 33.5%); γ: 4.74 (CV: 12.5%).

The predicted pharmacokinetic profiles by the established PBPK model well matched the observations both in plasma and tumor tissues of SGC-7901 tumor-bearing mice after single intravenous dose (6.25 mg/kg), with predictive fold-errors of all concentrations less than two (Figure 7B). It indicated that the developed PBPK model might desirably simulate pharmacokinetics of DPT in SGC-7901 xenograft models.

In vivo SGC-7901 tumor growth profiles during DPT administration were predicted based on the estimated in vitro pharmacodynamic parameters, simulated tumor concentration profiles and estimated tumor natural growth parameters (λ_0 = 0.257 day^{-1}, CV = 210%; λ_1 = 0.0589 mL/day, CV = 42.1%). The predicted profiles were consistent with observed data (Wang et al., 2015) (Figure 7C). All predicted relative tumor volumes fell within twofold errors (Figure 7D). The successful prediction further demonstrated the applicability of the developed PBPK-PD model in xenograft models.

DMD Fast Forward. Published on April 4, 2018 as DOI: 10.1124/dmd.117.079830
This article has not been copyedited and formatted. The final version may differ from this version.

Discussion

As a promising anti-tumor candidate, DPT shows potent cytotoxic effects both in vitro and in vivo. However, the intrinsic relationship between its in vitro and in vivo pharmacodynamics has not been explored. The main contribution of the present study was the development of a PBPK-PD model for revealing in vitro-in vivo pharmacodynamic correlation and predicting anti-tumor efficacy in tumor-bearing mice based on in vitro pharmacodynamics. The model approach was validated by multi-tumor model, indicating its potential application in anti-tumor drug discovery.

In general, in vitro anti-tumor activities of cytotoxic candidates like DPT are evaluated by static ways. Inhibition rates of cell proliferation following designed exposure times under different drug concentrations are obtained and IC_{50} values are estimated (Guerram et al., 2015; Jiang et al., 2013; Kim et al., 2002; Wu et al., 2013). By that approach, estimated IC_{50} values of DPT against NCI-H460 cell line varied from 7.51 to 9.40 nM in our study, depending on exposure time from 24 to 84 h. The parameter could not reflect the drug effect dynamically, and its variation might mislead our evaluation of the candidate. Therefore, a dynamic function quantitatively describing the cell count-time-concentration relationship of DPT was needed rather than a static one. There exist several in vitro dynamic models for cytotoxic compounds, including cell cycle specific/nonspecific model and transit compartment model (Jusko, 1971; Jusko, 1973; Mager and Jusko, 2001; Sun and Jusko, 1998). Since in vivo tumor growth usually doesn’t obey typical exponential feature, in vitro cycle specific/nonspecific model seemed not suitable to be extrapolated to in vivo circumstance. Our study also showed that although exponential model well described in vitro profiles, it unsatisfactorily characterized in vivo tumor growth. Time delay of the cytotoxic effect of DPT was not observed in our preliminary in vitro assays (data not shown), indicating that transit compartment model might also

DMD Fast Forward. Published on April 4, 2018 as DOI: 10.1124/dmd.117.079830
This article has not been copyedited and formatted. The final version may differ from this version.

not be proper. Consequently, we attempted a two-phase Koch model along with an inhibitive term related to the cytotoxic candidate, which could both dynamically reflect the anti-proliferation activity and be extended to predict in vivo pharmacodynamics. In vitro NCI-H460 cell proliferation was satisfactorily characterized by the model with stable estimations which were similar to the previous report (Wu et al., 2013).

Pharmacokinetic characteristics of DPT in NCI-H460 tumor-bearing mice were investigated. The estimated plasma CL values in tumor-bearing mice following two doses were similar (136.68 mL/min/kg for 6.25 mg/kg and 138.54 mL/min/kg for 25.0 mg/kg), but significantly higher than that in ICR mice (67.73 mL/min/kg for 25.0 mg/kg), accompanied with a higher distribution volume and a shorter half-life (Chen et al., 2016). It was also found that CL values of DPT in NCI-H460 tumor-bearing mice were larger than hepatic blood flow rate, demonstrating existence of extrahepatic elimination. However, this phenomenon did not occur in normal mice (Chen et al., 2016). We found that DPT was metabolic stable in both cultured NCI-H460 cells and homogenate of tumor tissue removed from NCI-H460 tumor-bearing mice, indicating that DPT metabolism did not occur in tumor. It is known that DPT is mainly metabolized by CYP2C family (Xie et al., 2016), which has an extensive distribution in extrahepatic tissues in murine (Graves et al., 2017; Tsao et al., 2001). Therefore, the extrahepatic elimination route might be urinary excretion or metabolism of extrahepatic CYP, which needed further investigation. The in vivo pharmacokinetic findings above indicated that tumor-bearing state might alter characteristics of DPT disposition. Further in vitro studies showed that tumor-bearing mice possessed higher intrinsic clearance in hepatic microsomes and lower plasma protein binding compared with normal mice (Chen et al., 2016; Xie et al., 2016). Higher intrinsic clearance in hepatic microsomes, lower plasma protein binding, high distribution in tumor tissue and

DMD Fast Forward. Published on April 4, 2018 as DOI: 10.1124/dmd.117.079830
This article has not been copyedited and formatted. The final version may differ from this version.

existence of extrahepatic elimination might all lead to the higher system clearance and distribution volume of DPT in tumor-bearing mice.

In vivo drug concentration perpetually varies following administration, which is distinguished from the constant level in culture medium. Therefore, a PBPK model established previously (Chen et al., 2016) was introduced to describe the dynamic profiles of DPT in tumor-bearing mice. It was noteworthy that concentration-time profiles in tumor did not synchronize with those in plasma. Although the mechanism leading to the accumulation of DPT in tumor tissue was unknown yet, the enhanced exposure at target site undoubtedly facilitated DPT to exert its anti-tumor efficacy. Since concentration profile in tumor tissue was obviously more meaningful for drug efficacy prediction than that in plasma, a tumor compartment was included in the PBPK model. It was found that pharmacokinetic profiles of DPT in tumor tissues were well characterized by permeability limited model rather than perfusion-rate limited model. It was noticed that mispredictions occurred to some extent in the normal tissues, although the predicted exposure ($AUC_{0\text{-}120min}$) in most of the tissues still fell within our twofold error criterion. In general, physiological parameters used in PBPK model for tumor-bearing mouse were considered similar to those for normal mice (Bradshaw-Pierce et al., 2008; Pawaskar et al., 2013; Zhang et al., 2013). In fact, tumor-bearing state may alter the physiological parameters and tissue properties, which may become reasons leading to misprediction. However, tumor concentration profiles which were associated with the anti-tumor effect directly were better predicted, with most of predicted concentrations falling within twofold error, indicating the established PBPK model was still acceptable (Guest et al., 2011; Parrott et al., 2005).

Pharmacokinetic profiles of DPT in tumor tissue during multi-dose DPT treatment were simulated by the developed PBPK model. It is worth mentioning that free drug concentration at the

DMD Fast Forward. Published on April 4, 2018 as DOI: 10.1124/dmd.117.079830
This article has not been copyedited and formatted. The final version may differ from this version.

target site may have a closer link with anti-tumor efficacy than total concentration. Therefore, unbound concentration profile of DPT in tumor tissue was considered into the model and supposed to directly account for the tumor growth inhibition. In order to predict the pharmacodynamics in tumor-bearing mice based on in vitro assays, in vivo pharmacodynamic model and parameters were considered the same as in vitro ones. In fact, we attempted to fit the in vivo model (equation 6) using perturbed tumor growth data of the present study and the estimated in vivo pharmacodynamic parameters (EC_{50}: 10.8 nM, E_{max}: 0.887 day^{-1} and γ: 7.00) turned out to be close to in vitro ones (EC_{50}: 8.97 nM, E_{max}: 0.820 day^{-1} and γ: 7.13), showing the consistency within in vitro and in vivo pharmacodynamics. To avoid accidental success, multifaceted in vivo observations were used to validate the efficacy prediction. For NCI-H460 xenograft model, predicted perturbed tumor growth curves desirably coincided with the observations of both present study and literature, although dosage regimens and natural growth parameters (λ_0 and λ_1) differed fundamentally between the two datasets, demonstrating the reliable and reasonable prediction of the model approach. What's more, the developed PBPK-PD model was further applied to predict perturbed tumor growth of SGC-7901 xenograft model from corresponding in vitro evaluations. It was consistent with our expectation that good prediction was obtained, indicating applicability of the proposed model. Pharmacodynamic characteristics and mechanisms of a cytotoxic compound seemed constant between in vitro and in vivo assays of the same cell line, making it possible to predict in vivo anti-tumor efficacy from in vitro studies, which remained to be further validated by other compounds.

Although many reports demonstrated the applications of PK-PD or PBPK-PD model on anti-tumor agents, almost all of them focused on either in vitro or in vivo assays alone (Del Bene et al., 2009; Lobo and Balthasar, 2002; Nanavati and Mager, 2017; Yuan et al., 2015). Those reports

DMD Fast Forward. Published on April 4, 2018 as DOI: 10.1124/dmd.117.079830
This article has not been copyedited and formatted. The final version may differ from this version.

developed in vitro or in vivo models separately and seldom related them together, let alone predicted in vivo efficacy based on in vitro assays. In our study, we established a novel in vitro pharmacodynamic model which was able to be extended to predict in vivo efficacy, and subsequently proposed a PBPK-PD model approach to achieve the prediction, which was validated by datasets from multi-source. To our knowledge, this was the first time to obtain desirable prediction of in vivo anti-tumor efficacy of a candidate based on its in vitro evaluation through PBPK-PD model establishment. Natural growth parameters (λ_0 and λ_1) of targeted tumor were still needed during the prediction, but they might be derived from databases instead. The proposed predictive approach could help dosage regimen design in the stage of in vivo evaluation, when in vitro pharmacodynamic data were available. In addition, facing quantities of candidates with different anti-tumor activity levels in early phase of drug discovery, the present approach might help to rapidly predict their in vivo efficacy and screen out the most promising ones or sensitive tumor types, thus accelerating the discovery process.

In summary, the quantitatively extended preclinical evaluations of DPT deepened our understanding of the links existing between in vitro and in vivo pharmacodynamics. We proposed a predictive PBPK-PD model approach, by which anti-tumor efficacy of DPT in tumor-bearing mice was successfully predicted based on in vitro pharmacodynamics, indicating that in vitro cytotoxic assays and quantitative models might play significant roles in forecasting in vivo anti-tumor efficacy.

DMD Fast Forward. Published on April 4, 2018 as DOI: 10.1124/dmd.117.079830
This article has not been copyedited and formatted. The final version may differ from this version.

Acknowledgments

We thank Jiangsu Key Laboratory of Carcinogenesis and Intervention for the kind supports to the feeding and experiments of tumor-bearing mice.

DMD Fast Forward. Published on April 4, 2018 as DOI: 10.1124/dmd.117.079830
This article has not been copyedited and formatted. The final version may differ from this version.

Authorship Contributions

Participated in research design: Chen, Zhao, L. Liu, and X.D. Liu.

Conducted experiments: Chen, Zhao, F. Liu, Li, and Hong.

Contributed new reagents or analytic tools: F. Liu, Li, and Hong.

Performed data analysis: Chen, Zhao, Zhong, and X.D. Liu.

Wrote or contributed to the writing of the manuscript: Chen, Zhao, Li, Zhong, and L. Liu.

References

Bradshaw-Pierce EL, Steinhauer CA, Raben D, and Gustafson DL (2008) Pharmacokinetic-directed dosing of vandetanib and docetaxel in a mouse model of human squamous cell carcinoma. *Mol Cancer Ther* **7**(9)**:** 3006-3017.

Chen GM, Hu N, Liu L, Xie SS, Wang P, Li J, Xie L, Wang GJ, and Liu XD (2011) Pharmacokinetics of verapamil in diabetic rats induced by combination of high-fat diet and streptozotocin injection. *Xenobiotica* **41**(6)**:** 494-500.

Chen Y, Zhao K, Liu F, Xie Q, Zhong Z, Miao M, Liu X, and Liu L (2016) Prediction of Deoxypodophyllotoxin Disposition in Mouse, Rat, Monkey, and Dog by Physiologically Based Pharmacokinetic Model and the Extrapolation to Human. *Front Pharmacol* **7:** 488.

Del Bene F, Germani M, De Nicolao G, Magni P, Re CE, Ballinari D, and Rocchetti M (2009) A model-based approach to the in vitro evaluation of anticancer activity. *Cancer Chemother Pharmacol* **63**(5)**:** 827-836.

Eigenmann MJ, Frances N, Hoffmann G, Lave T, and Walz AC (2016) Combining Nonclinical Experiments with Translational PKPD Modeling to Differentiate Erlotinib and Gefitinib. *Mol Cancer Ther* **15**(12)**:** 3110-3119.

Graves JP, Gruzdev A, Bradbury JA, DeGraff LM, Edin ML, and Zeldin DC (2017) Characterization of the Tissue Distribution of the Mouse Cyp2c Subfamily by Quantitative PCR Analysis. *Drug Metab Dispos* **45**(7)**:** 807-816.

Guerram M, Jiang ZZ, Sun L, Zhu X, and Zhang LY (2015) Antineoplastic effects of deoxypodophyllotoxin, a potent cytotoxic agent of plant origin, on glioblastoma U-87 MG and SF126 cells. *Pharmacol Rep* **67**(2)**:** 245-252.

Guest EJ, Aarons L, Houston JB, Rostami-Hodjegan A, and Galetin A (2011) Critique of the two-fold measure of prediction success for ratios: application for the assessment of drug-drug interactions. *Drug Metab Dispos* **39**(2)**:** 170-173.

Hu S, Zhou Q, Wu WR, Duan YX, Gao ZY, Li YW, and Lu Q (2016) Anticancer effect of deoxypodophyllotoxin induces apoptosis of human prostate cancer cells. *Oncol Lett* **12**(4)**:** 2918-2923.

Jiang Z, Wu M, Miao J, Duan H, Zhang S, Chen M, Sun L, Wang Y, Zhang X, Zhu X, and Zhang L (2013) Deoxypodophyllotoxin exerts both anti-angiogenic and vascular disrupting effects. *Int J Biochem Cell Biol* **45**(8)**:** 1710-1719.

Jusko WJ (1971) Pharmacodynamics of chemotherapeutic effects: dose-time-response relationships for phase-nonspecific agents. *J Pharm Sci* **60**(6)**:** 892-895.

Jusko WJ (1973) A pharmacodynamic model for cell-cycle-specific chemotherapeutic agents. *J Pharmacokinet Biopharm* **1:** 175-200.

Kelland LR (2004) Of mice and men: values and liabilities of the athymic nude mouse model in anticancer drug development. *Eur J Cancer* **40**(6)**:** 827-836.

Khaled M, Belaaloui G, Jiang ZZ, Zhu X, and Zhang LY (2016) Antitumor effect of Deoxypodophyllotoxin on human breast cancer xenograft transplanted in BALB/c nude mice model. *J Infect Chemother* **22**(10)**:** 692-696.

Khaled M, Jiang ZZ, and Zhang LY (2013) Deoxypodophyllotoxin: a promising therapeutic agent from herbal medicine. *J Ethnopharmacol* **149**(1)**:** 24-34.

Kim Y, Kim SB, You YJ, and Ahn BZ (2002) Deoxypodophyllotoxin; the cytotoxic and antiangiogenic component from Pulsatilla koreana. *Planta Med* **68**(3)**:** 271-274.

Koch G, Walz A, Lahu G, and Schropp J (2009) Modeling of tumor growth and anticancer effects of combination therapy. *J Pharmacokinet Pharmacodyn* **36**(2)**:** 179-197.

Liu F, Chen Y, Xie QS, Liu L, Xu P, Zhong ZY, and Liu XD (2016) Simultaneous Determination of Deoxypodophyllotoxin and Its Major Metabolites in Rat Plasma by a Sensitive LC-MS/MS Method and Its Application in a Pharmacokinetic Study. *Chromatographia* **79**(1-2)**:** 53-61.

Lobo ED and Balthasar JP (2002) Pharmacodynamic modeling of chemotherapeutic effects: application of a transit compartment model to characterize methotrexate effects in vitro. *AAPS PharmSci* **4**(4)**:** E42.

Mager DE and Jusko WJ (2001) Pharmacodynamic modeling of time-dependent transduction systems. *Clin Pharmacol Ther* **70**(3)**:** 210-216.

Magni P, Simeoni M, Poggesi I, Rocchetti M, and De Nicolao G (2006) A mathematical model to study the effects of drugs administration on tumor growth dynamics. *Math Biosci* **200**(2)**:** 127-151.

Maurer TS, Debartolo DB, Tess DA, and Scott DO (2005) Relationship between exposure and nonspecific binding of thirty-three central nervous system drugs in mice. *Drug Metab Dispos* **33**(1)**:** 175-181.

Nanavati C and Mager DE (2017) Sequential Exposure of Bortezomib and Vorinostat is Synergistic in Multiple Myeloma Cells. *Pharm Res* **34**(3)**:** 668-679.

Parrott N, Paquereau N, Coassolo P, and Lave T (2005) An evaluation of the utility of physiologically based models of pharmacokinetics in early drug discovery. *J Pharm Sci* **94**(10)**:** 2327-2343.

Pawaskar DK, Straubinger RM, Fetterly GJ, Hylander BH, Repasky EA, Ma WW, and Jusko WJ (2013) Physiologically based pharmacokinetic models for everolimus and sorafenib in mice.

Cancer Chemother Pharmacol **71**(5)**:** 1219-1229.

Ruggeri BA, Camp F, and Miknyoczki S (2014) Animal models of disease: pre-clinical animal models of cancer and their applications and utility in drug discovery. *Biochem Pharmacol* **87**(1)**:** 150-161.

Salphati L, Wong H, Belvin M, Bradford D, Edgar KA, Prior WW, Sampath D, and Wallin JJ (2010) Pharmacokinetic-pharmacodynamic modeling of tumor growth inhibition and biomarker modulation by the novel phosphatidylinositol 3-kinase inhibitor GDC-0941. *Drug Metab Dispos* **38**(9)**:** 1436-1442.

Shin SY, Yong Y, Kim CG, Lee YH, and Lim Y (2010) Deoxypodophyllotoxin induces G2/M cell cycle arrest and apoptosis in HeLa cells. *Cancer Lett* **287**(2)**:** 231-239.

Sun YN and Jusko WJ (1998) Transit compartments versus gamma distribution function to model signal transduction processes in pharmacodynamics. *J Pharm Sci* **87**(6)**:** 732-737.

Tsao CC, Coulter SJ, Chien A, Luo G, Clayton NP, Maronpot R, Goldstein JA, and Zeldin DC (2001) Identification and localization of five CYP2Cs in murine extrahepatic tissues and their metabolism of arachidonic acid to regio- and stereoselective products. *J Pharmacol Exp Ther* **299**(1)**:** 39-47.

Wang YR, Xu Y, Jiang ZZ, Guerram M, Wang B, Zhu X, and Zhang LY (2015) Deoxypodophyllotoxin induces G2/M cell cycle arrest and apoptosis in SGC-7901 cells and inhibits tumor growth in vivo. *Molecules* **20**(1)**:** 1661-1675.

Wong SK, Tsui SK, Kwan SY, Su XL, and Lin RC (2000) Identification and characterization of Podophyllum emodi by API-LC/MS/MS. *J Mass Spectrom* **35**(11)**:** 1246-1251.

Wu M, Jiang Z, Duan H, Sun L, Zhang S, Chen M, Wang Y, Gao Q, Song Y, Zhu X, and Zhang L

(2013) Deoxypodophyllotoxin triggers necroptosis in human non-small cell lung cancer NCI-H460 cells. *Biomed Pharmacother* **67**(8)**:** 701-706.

Xie Q, Chen Y, Liu F, Zhong Z, Zhao K, Ling Z, Wang F, Tang X, Wang Z, Liu L, and Liu X (2016) Interspecies differences in metabolism of deoxypodophyllotoxin in hepatic microsomes from human, monkey, rat, mouse and dog. *Drug Metab Pharmacokinet* **31**(4)**:** 314-322.

Yong Y, Shin SY, Lee YH, and Lim Y (2009) Antitumor activity of deoxypodophyllotoxin isolated from Anthriscus sylvestris: Induction of G2/M cell cycle arrest and caspase-dependent apoptosis. *Bioorg Med Chem Lett* **19**(15)**:** 4367-4371.

Yuan Y, Zhou X, Ren Y, Zhou S, Wang L, Ji S, Hua M, Li L, Lu W, and Zhou T (2015) Semi-Mechanism-Based Pharmacokinetic/Pharmacodynamic Model for the Combination Use of Dexamethasone and Gemcitabine in Breast Cancer. *J Pharm Sci* **104**(12)**:** 4399-4408.

Zhang T, Li Y, Zou P, Yu JY, McEachern D, Wang S, and Sun D (2013) Physiologically based pharmacokinetic and pharmacodynamic modeling of an antagonist (SM-406/AT-406) of multiple inhibitor of apoptosis proteins (IAPs) in a mouse xenograft model of human breast cancer. *Biopharm Drug Dispos* **34**(6)**:** 348-359.

Footnotes

The project was supported by the National Natural Science Foundation of China [No. 81673505, 81573490]; the Natural Science Foundation of Jiangsu Province of China [BK20161457]; and the Priority Academic Program Development of Jiangsu Higher Education Institutions and the Policy Directive Program of Jiangsu Province [BY2015072-03].

Reprint requests:

Li Liu (liulee@yeah.net)

Center of Drug Metabolism and Pharmacokinetics, School of Pharmacy, China Pharmaceutical University, No.24 Tongjia Lane, Nanjing 210009, China.

[1]Yang Chen and Kaijing Zhao are co-first authors.

[2]Xiaodong Liu and Li Liu are co-corresponding authors.

DMD Fast Forward. Published on April 4, 2018 as DOI: 10.1124/dmd.117.079830
This article has not been copyedited and formatted. The final version may differ from this version.

Figure Legends

Figure 1. Schematic diagram of PBPK model of DPT in tumor-bearing mouse. a and b represent vascular and extravascular compartment, respectively. CL_{other} represents clearance of extrahepatic elimination. Q and solid arrows represent blood flow. GIT and ROB represent gastrointestinal tract and rest of body, respectively.

Figure 2. The calibration curves to determine cultured NCI-H460 cell counts on five consecutive days.

Figure 3. The observed (symbol) and fitted (line) proliferation profiles of NCI-H460 cells under various concentrations of DPT by cell cycle non-specific cytotoxicity model (A) and the cytotoxicity model extended from two-phase Koch model (B). Symbols represent mean±SD (n=5) of cell counts determined by calibration curves.

Figure 4. Observed (symbol) and predicted (line) concentration-time profiles of DPT by the developed PBPK model in plasma (A) and tumor (B) of NCI-H460 tumor-bearing mice following single intravenous dose. Symbols represent mean±SD (n=6) of observations. (C) represents the relationship between mean observed and predicted DPT concentrations in plasma and tumor of the two dose groups above at each time point, where solid and dashed lines indicate unity and twofold errors of prediction, respectively.

Figure 5. Observed (symbol) and predicted (line) concentration-time profiles of DPT by the

DMD Fast Forward. Published on April 4, 2018 as DOI: 10.1124/dmd.117.079830
This article has not been copyedited and formatted. The final version may differ from this version.

developed PBPK model in heart (A), liver (B), lung (C), kidney (D), brain (E), muscle (F) and gastrointestinal tract (G) of NCI-H460 tumor-bearing mice following single intravenous dose (25 mg/kg). Symbols represent mean±SD (n=6) of observations. (H) represents the relationship between observed and predicted $AUC_{0\text{-}120min}$ of DPT in the tissues above, where solid and dashed lines indicate unity and twofold errors of prediction, respectively.

Figure 6. PBPK-PD model prediction in NCI-H460 tumor-bearing mice.

(A) and (B): Observed (symbol) and predicted (line) profiles of tumor growth by the developed PBPK-PD model in NCI-H460 tumor-bearing mice during multiple intravenous doses of DPT treatment (A: every three days; B: three times a week). Symbols represent mean±SD of observations (A: n=6; B: n=12 or 6) which came from the present (A) and previous (B) study (Wu et al., 2013). The day of first administration was designated as time zero.

(C) and (D): The relationship between mean observed and predicted tumor volumes at each time point in (A) and (B) above, respectively, where solid and dashed lines indicate unity and twofold errors of prediction, respectively.

Figure 7. PBPK-PD model application in SGC-7901 tumor-bearing mice.

(A): The observed (symbol) and fitted (line) proliferation profiles of SGC-7901 cells under various concentrations of DPT by the cytotoxicity model extended from two-phase Koch model. Symbols represent mean±SD (n=5) of cell counts determined by calibration curves.

(B): Observed (symbol) and predicted (line) concentration-time profiles of DPT by the developed PBPK model in plasma and tumor of SGC-7901 tumor-bearing mice following single intravenous

DMD Fast Forward. Published on April 4, 2018 as DOI: 10.1124/dmd.117.079830
This article has not been copyedited and formatted. The final version may differ from this version.

dose of 6.25 mg/kg. Symbols represent mean±SD (n=3) of observations. The inset is the relationship between mean observed and predicted DPT concentrations in plasma and tumor of SGC-7901 tumor-bearing mice at each time point, where solid and dashed lines indicate unity and twofold errors of prediction, respectively.

(C): Observed (symbol) and predicted (line) profiles of tumor growth by the developed PBPK-PD model in SGC-7901 tumor-bearing mice during multiple intravenous doses of DPT treatment (three times a week). Symbols represent mean±SD (n=6) of observations which came from the previous study (Wang et al., 2015). The day of first administration was designated as time zero.

(D): The relationship between mean observed and predicted relative tumor volumes at each time point in (C), where solid and dashed lines indicate unity and twofold errors of prediction, respectively.

DMD Fast Forward. Published on April 4, 2018 as DOI: 10.1124/dmd.117.079830
This article has not been copyedited and formatted. The final version may differ from this version.

Tables

Table 1. Physiological parameters for tumor-bearing mouse (20 g) used in PBPK model.

	Volume[a] (mL)	Blood flow rate[a] (mL/min)	$K_{p,T}$[b]
Adipose	1.73	0.72	19.59
Liver	1.10	1.94	1.52
Muscle	7.67	0.91	0.68
Lungs	0.15	8.14 (Cardiac output)	1.55
Kidneys	0.33	1.30	1.28
Brain	0.33	0.26	2.51
Heart	0.10	0.28	0.88
Spleen	0.07	0.09	0.96
Skin	3.30	0.41	1.29
Gastrointestinal tract	0.85	1.50	0.91
Tumor[c]	0.50	0.14	4.23
Rest of body	3.39	2.18	0.0090
Vein	0.65	\	\
Artery	0.33	\	\

[a] Volumes and blood flow rates of normal tissues were cited from the previous report (Chen et al., 2016).

[b] $K_{p,T}$ of normal tissues were calculated from the values of rat ($K_{p,T,rat}$) (Chen et al., 2016) based on the equation $K_{p,T} = K_{p,T,rat} \cdot f_u / f_{u,rat}$, where f_u and $f_{u,rat}$ mean unbound fraction of DPT in plasma of

DMD Fast Forward. Published on April 4, 2018 as DOI: 10.1124/dmd.117.079830
This article has not been copyedited and formatted. The final version may differ from this version.

tumor-bearing mouse and rat, respectively.

[c] Tumor volume came from the actual volume. Blood flow rate of tumor was cited from the previous report (Zhang et al., 2013). $K_{p,T}$ value of tumor was calculated from the $AUC_{0-\infty}$ ratio between tumor tissue and plasma of 6.25 mg/kg single intravenous dose group.

DMD Fast Forward. Published on April 4, 2018 as DOI: 10.1124/dmd.117.079830
This article has not been copyedited and formatted. The final version may differ from this version.

Table 2. Estimated in vitro pharmacodynamic parameters of DPT against NCI-H460 cell line using cell cycle non-specific cytotoxicity model (A) and the cytotoxicity model extended from two-phase Koch model (B). Data in parentheses denote corresponding CV.

	Model A	Model B
k_{ng} (day^{-1})	0.905 (1.56%)	\
λ_0 (day^{-1})	\	0.521 (2.73%)
λ_1 (count/day)	\	3.08×10^5 (17.8%)
EC_{50} (nM)	9.07 (1.04%)	8.97 (0.864%)
E_{max} (day^{-1})	0.775 (2.53%)	0.820 (2.04%)
γ	7.16 (3.10%)	7.13 (2.68%)

DMD Fast Forward. Published on April 4, 2018 as DOI: 10.1124/dmd.117.079830
This article has not been copyedited and formatted. The final version may differ from this version.

Table 3. Comparison of pharmacokinetic parameters of DPT in plasma and tumor of NCI-H460 tumor-bearing mice following single intravenous dose estimated from observed (Obs) and predicted (Pred) concentration-time profiles by the developed PBPK model.

		Plasma		Tumor	
		6.25 mg/kg	25 mg/kg	6.25 mg/kg	25 mg/kg
$AUC_{0\text{-}tn}$ (μM·min)	Obs	108.47	449.85	428.62	1387.99
	Pred	86.11	440.68	490.05	2322.46
$AUC_{0\text{-}\infty}$ (μM·min)	Obs	114.90	453.42	485.60	1720.75
	Pred	90.30	443.84	531.81	2520.70
CL (mL/min/kg)	Obs	136.68	138.54	/	/
	Pred	173.91	141.52	/	/
V_{ss} (L/kg)	Obs	3.30	3.53	/	/
	Pred	4.06	3.33	/	/
$t_{1/2}$ (min)	Obs	51.21	43.96	156.96	204.67
	Pred	41.83	43.60	126.38	126.38
C_{max} (μM)	Obs	/	/	2.59	15.67
	Pred	/	/	2.18	10.33

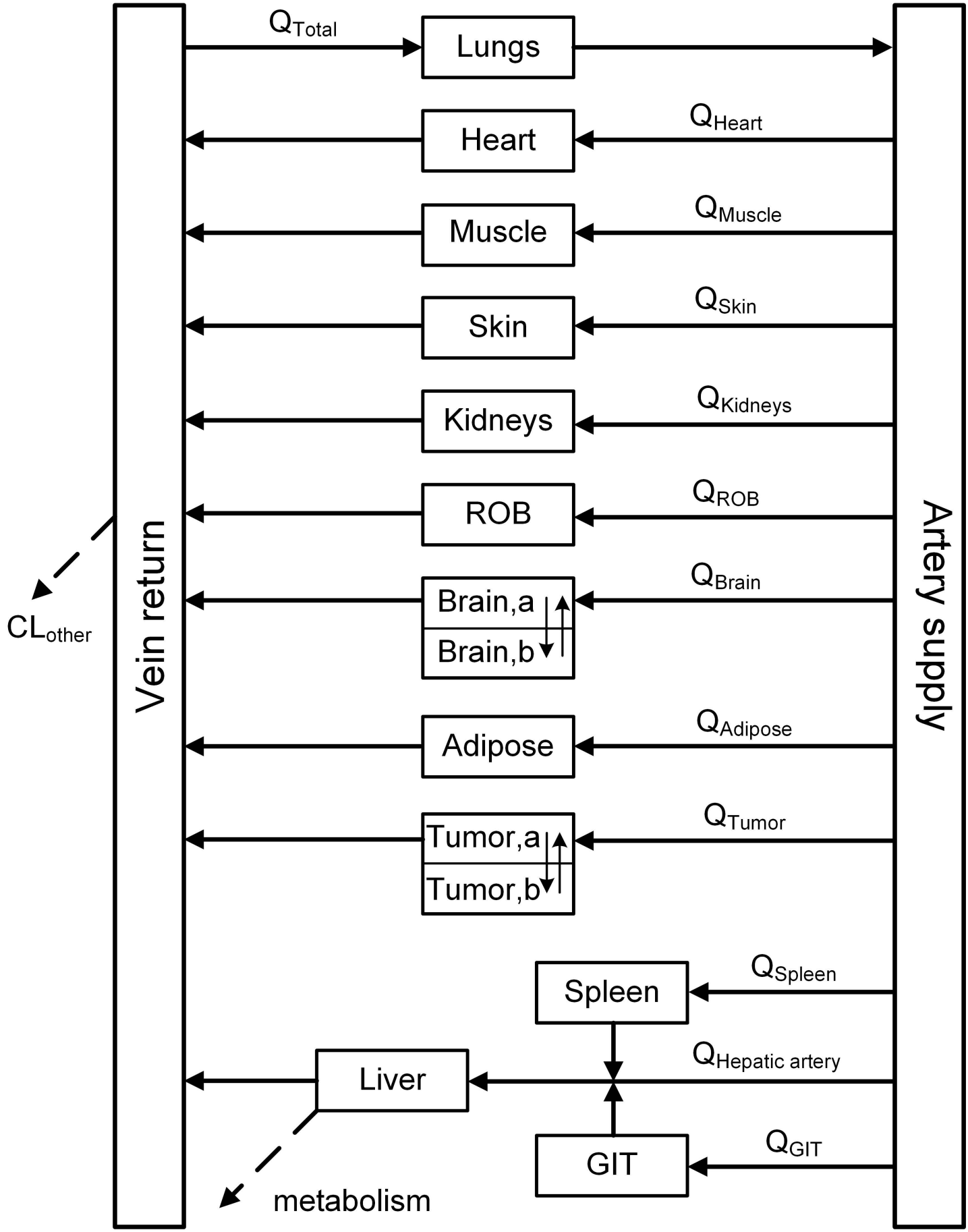
Q_{Total}
Lungs
Heart
Q_{Heart}
Muscle
Q_{Muscle}
Skin
Q_{Skin}
Kidneys
$Q_{Kidneys}$
ROB
Q_{ROB}
Brain,a
Brain,b
Q_{Brain}
Adipose
$Q_{Adipose}$
Tumor,a
Tumor,b
Q_{Tumor}
Spleen
Q_{Spleen}
Liver
$Q_{Hepatic\ artery}$
GIT
Q_{GIT}
CL_{other}
metabolism
Vein return
Artery supply

Fig.1

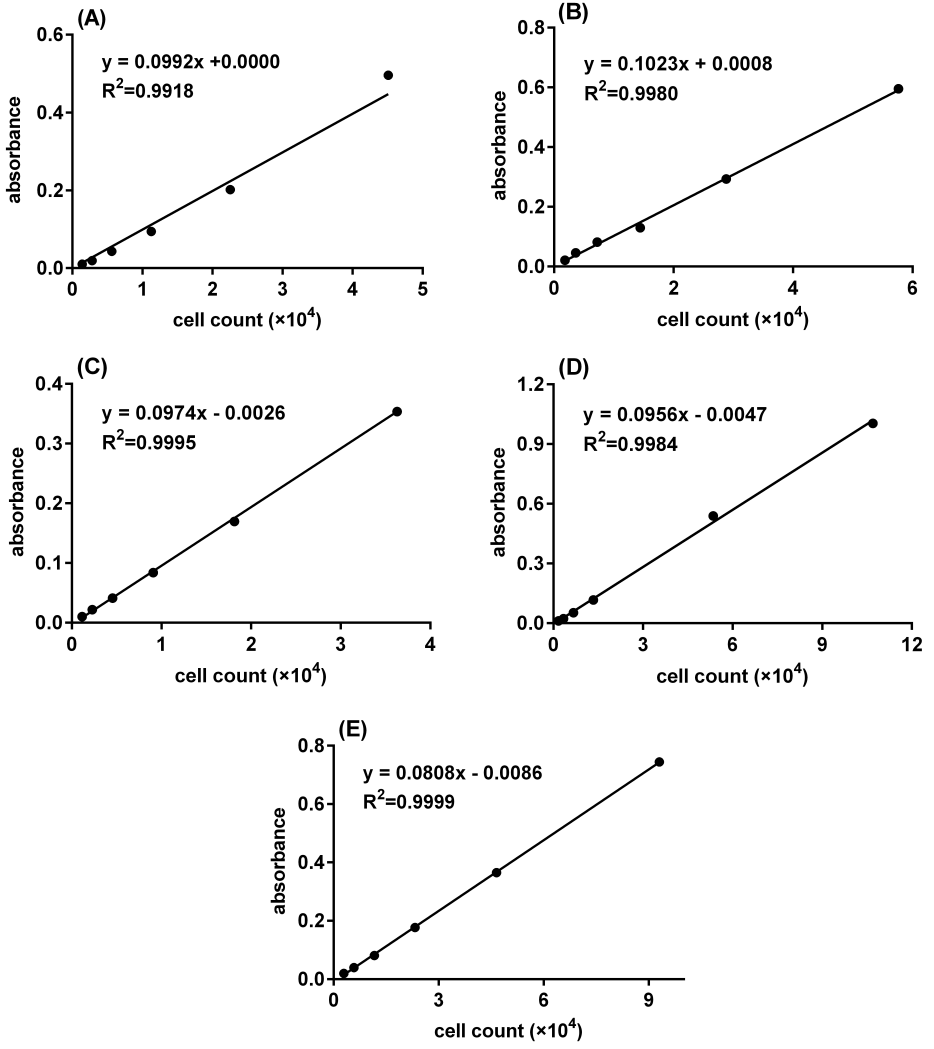
(A)
y = 0.0992x +0.0000
R2=0.9918
absorbance
cell count (×10^4)
(B)
y = 0.1023x + 0.0008
R2=0.9980
absorbance
cell count (×10^4)
(C)
y = 0.0974x - 0.0026
R2=0.9995
absorbance
cell count (×10^4)
(D)
y = 0.0956x - 0.0047
R2=0.9984
absorbance
cell count (×10^4)
(E)
y = 0.0808x - 0.0086
R2=0.9999
absorbance
cell count (×10^4)

Fig. 2

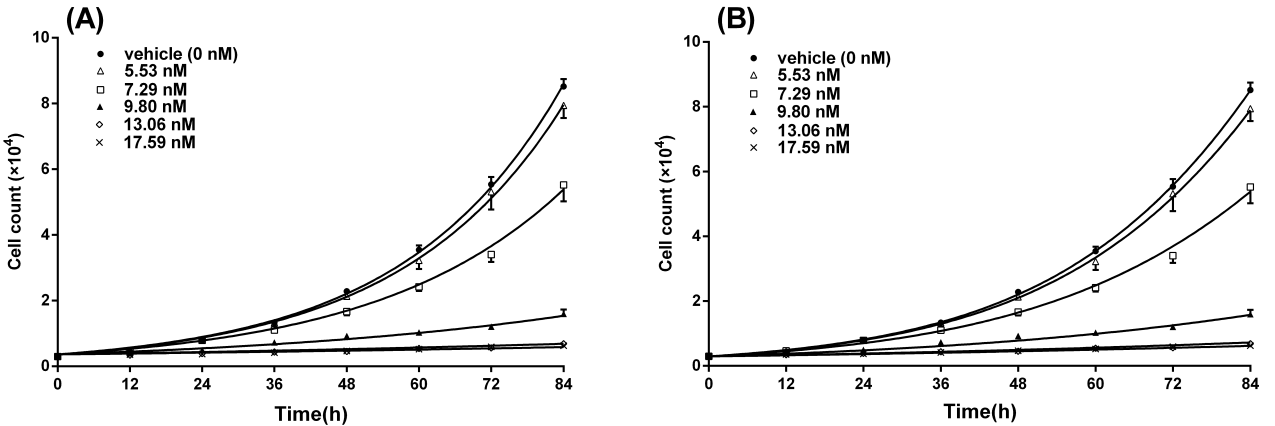
(A)
vehicle (0 nM)
5.53 nM
7.29 nM
9.80 nM
13.06 nM
17.59 nM
Cell count (×10⁴)
Time(h)
0
12
24
36
48
60
72
84
2
4
6
8
10
(B)
vehicle (0 nM)
5.53 nM
7.29 nM
9.80 nM
13.06 nM
17.59 nM
Cell count (×10⁴)
Time(h)

Fig. 3

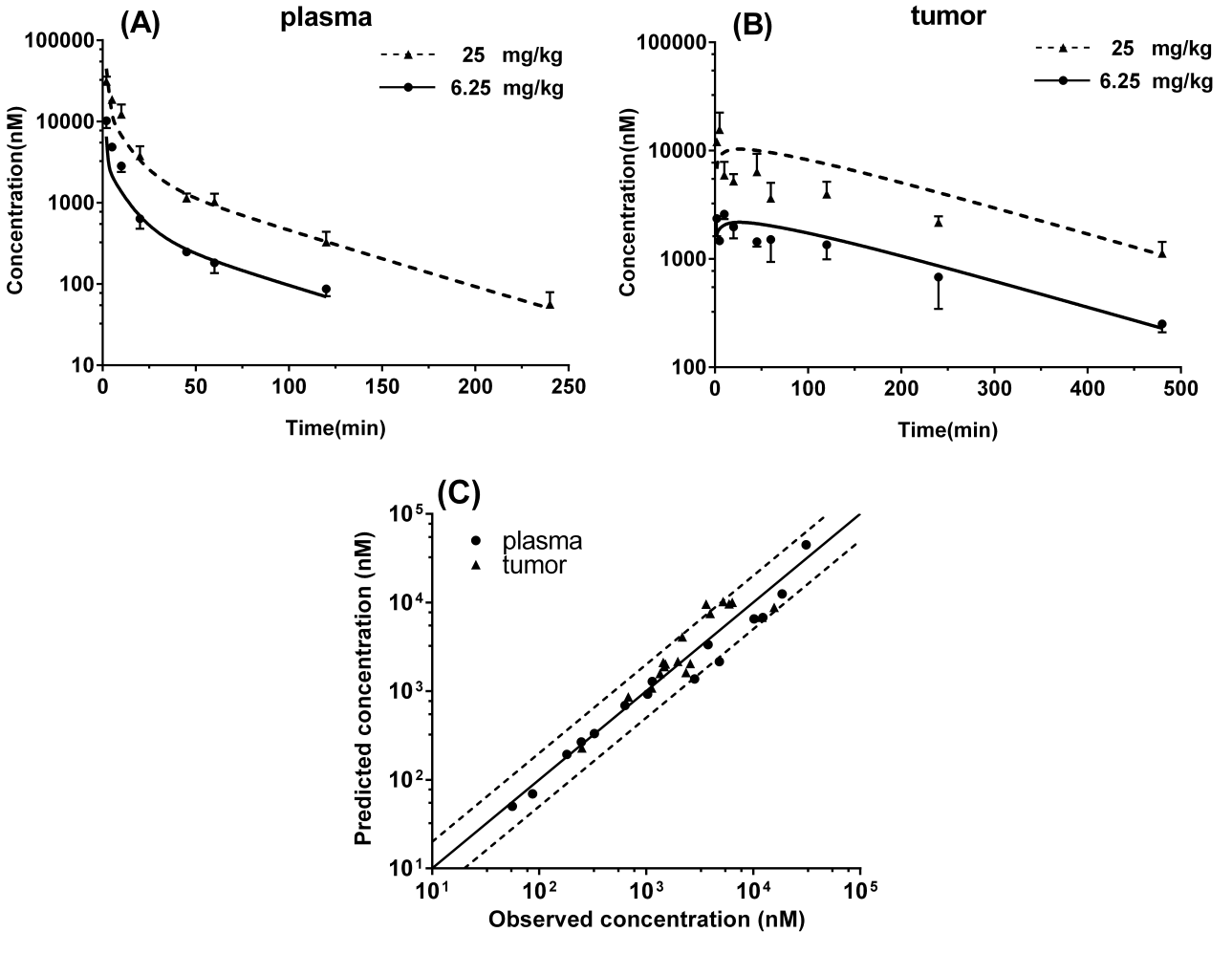
(A)
plasma
25 mg/kg
6.25 mg/kg
Concentration(nM)
Time(min)
(B)
tumor
25 mg/kg
6.25 mg/kg
Concentration(nM)
Time(min)
(C)
plasma
tumor
Predicted concentration (nM)
Observed concentration (nM)

Fig. 4

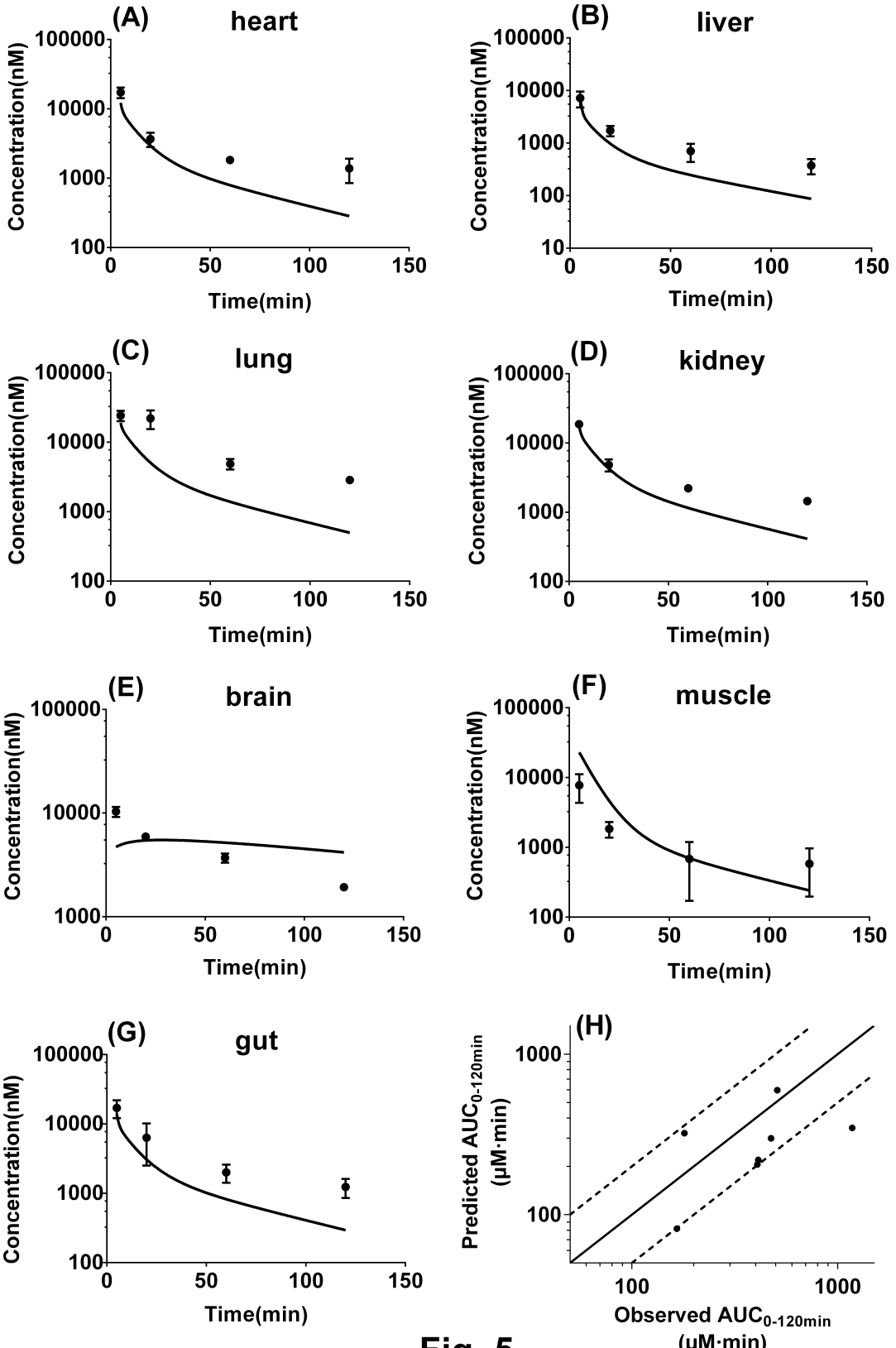
(A)
heart
Concentration(nM)
Time(min)
(B)
liver
Concentration(nM)
Time(min)
(C)
lung
Concentration(nM)
Time(min)
(D)
kidney
Concentration(nM)
Time(min)
(E)
brain
Concentration(nM)
Time(min)
(F)
muscle
Concentration(nM)
Time(min)
(G)
gut
Concentration(nM)
Time(min)
(H)
Predicted AUC0-120min (μM·min)
Observed AUC0-120min (μM·min)

Fig. 5

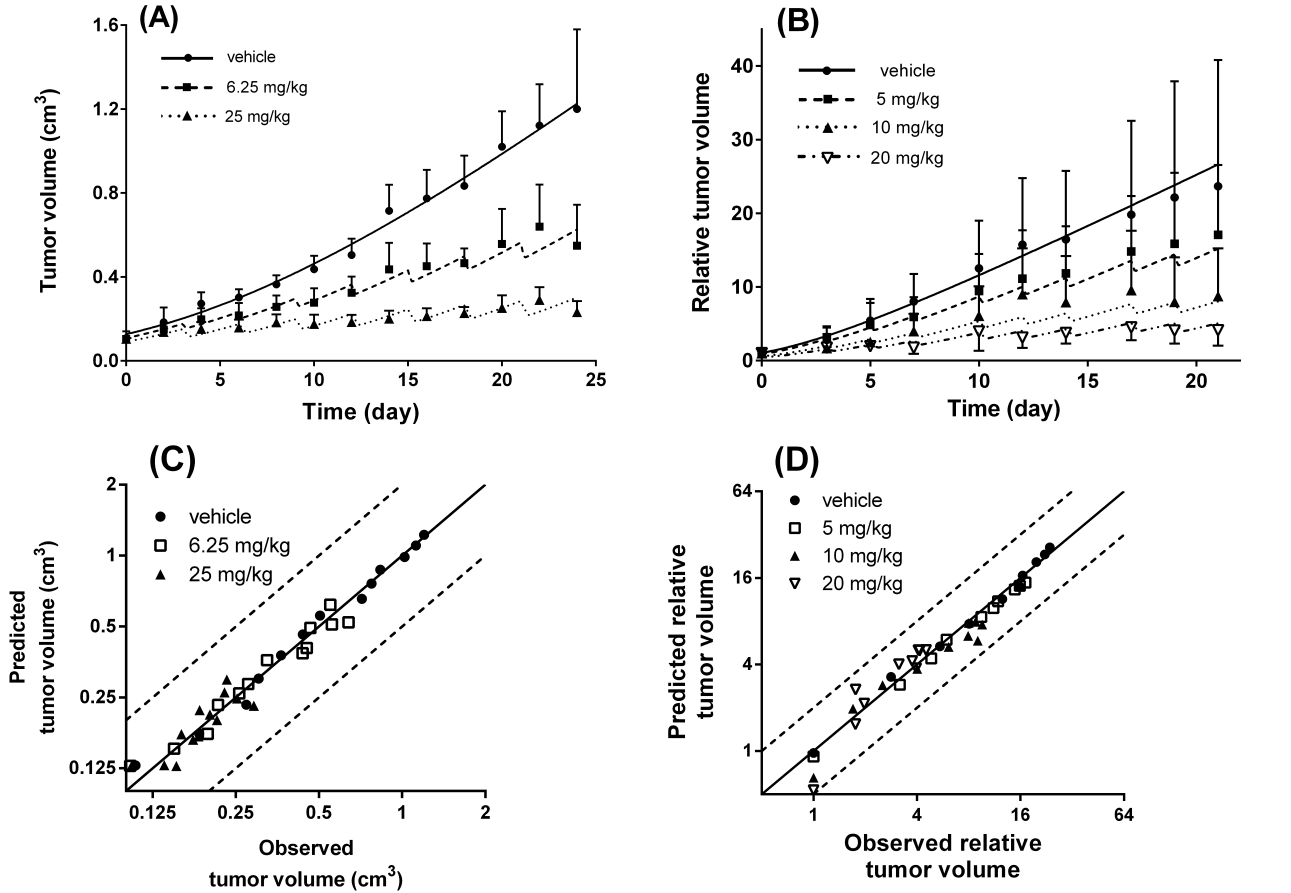
(A)
vehicle
6.25 mg/kg
25 mg/kg
Tumor volume (cm3)
Time (day)
(B)
vehicle
5 mg/kg
10 mg/kg
20 mg/kg
Relative tumor volume
Time (day)
(C)
vehicle
6.25 mg/kg
25 mg/kg
Predicted tumor volume (cm3)
Observed tumor volume (cm3)
(D)
vehicle
5 mg/kg
10 mg/kg
20 mg/kg
Predicted relative tumor volume
Observed relative tumor volume

Fig.6

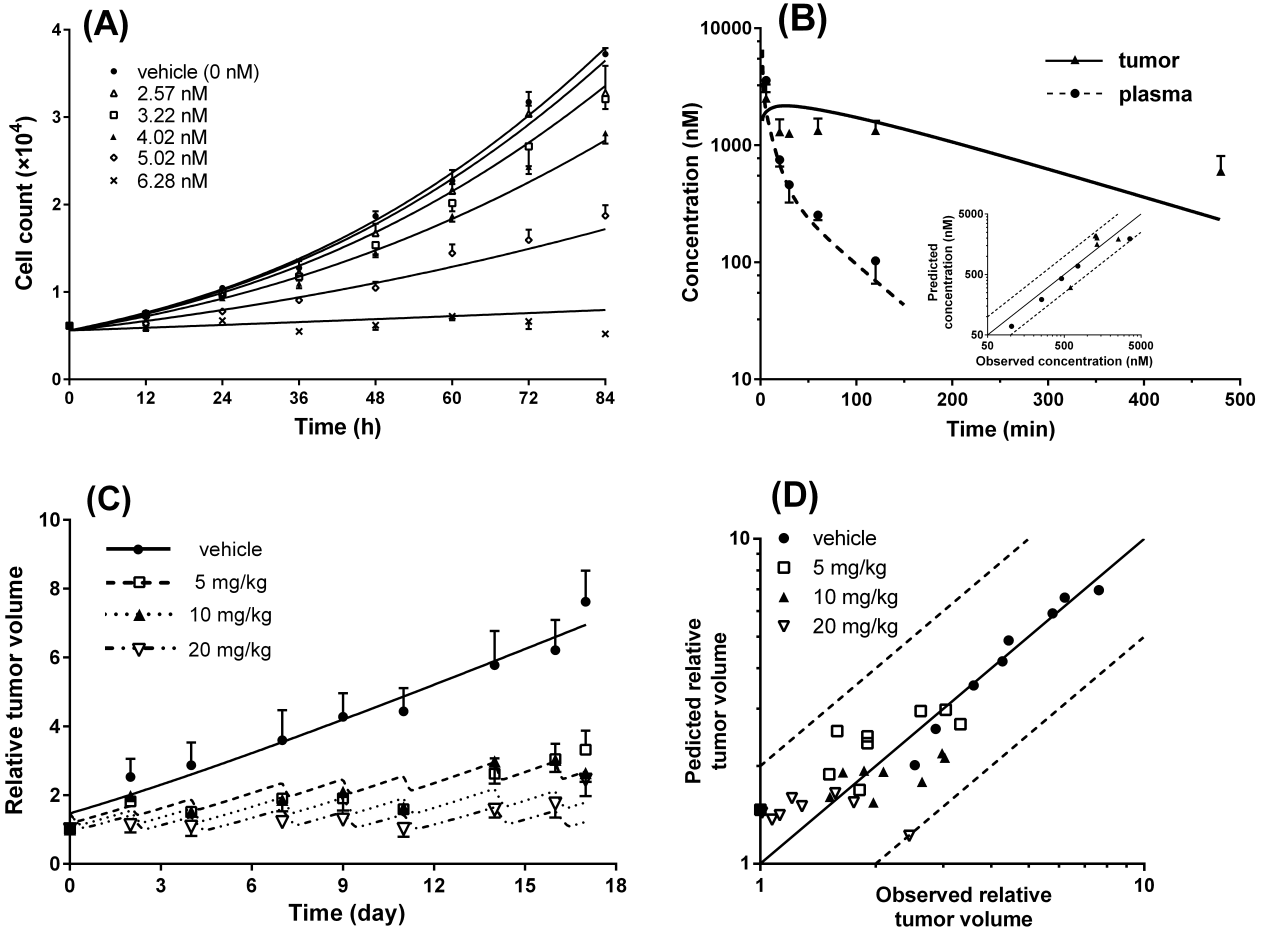
(A)
vehicle (0 nM)
2.57 nM
3.22 nM
4.02 nM
5.02 nM
6.28 nM
Cell count (×10^4)
Time (h)
(B)
tumor
plasma
Concentration (nM)
Time (min)
Predicted concentration (nM)
Observed concentration (nM)
(C)
vehicle
5 mg/kg
10 mg/kg
20 mg/kg
Relative tumor volume
Time (day)
(D)
vehicle
5 mg/kg
10 mg/kg
20 mg/kg
Pedicted relative tumor volume
Observed relative tumor volume

Fig.7